Combined time-resolved x-ray magnetic circular dichroism and ferromagnetic resonance studies of magnetic alloys and multilayers (invited)

D. A. Arena,[a] E. Vescovo, and C.-C. Kao
National Synchrotron Light Source, Brookhaven National Laboratory, Upton, New York 11973

Y. Guan and W. E. Bailey
Materials Science Program, Department of Applied Physics, Columbia University, New York, New York 10027

(Presented on 8 January 2007; received 31 October 2006; accepted 19 December 2006; published online 3 May 2007)

We present measurements of element- and time-resolved ferromagnetic resonance (FMR) in magnetic thin films at gigahertz frequencies via an implementation of time-resolved x-ray magnetic circular dichroism (TR-XMCD). By combining TR-XMCD and FMR, using a rf excitation that is phase locked to the photon bunch clock, the dynamic response of individual layers or precession of individual elements in an alloy can be measured. The technique also provides extremely accurate measurements of the precession cone angle (to 0.1°) and the phase of oscillation (to 2°, or ~5 ps at 2.3 GHz). TR-XMCD combined with FMR can be used to study the origins of precessional damping by measuring the relative phase of dissimilar precessing magnetic moments. We have used the technique to measure the response of specific elements and separate layers in several alloys and structures, including a single $Ni_{81}Fe_{19}$ layer, a pseudo-spin-valve structure ($Ni_{81}Fe_{19}/Cu/Co_{93}Zr_7$), magnetic bilayers consisting of low damping ($Co_{93}Zr_7$) and high damping (Tb-doped $Ni_{81}Fe_{19}$) layers joined across a common interface, and elemental moments in Tb-doped $Ni_{81}Fe_{19}$. © *2007 American Institute of Physics*. [DOI: 10.1063/1.2712294]

I. INTRODUCTION

Ferromagnetic resonance (FMR) has been used extensively to determine fundamental parameters that affect magnetism in thin films.[1] The success of FMR in revealing the resonance frequencies (related to internal and applied fields) and relaxation (determined by damping of the resonance) illustrates the usefulness of the technique.[2] However, the growing complexity of many modern FM materials and devices, for example, structures in which sophisticated, materials-based techniques are used to control precession relaxation and resonance frequencies, provides an impetus to develop measurement techniques that reveal, in a more direct fashion, the microscopic origin of relevant interactions.[3–6]

In this article, we present element- and time-resolved measurements of ferromagnetic resonance in thin film alloys,[7] a pseudo-spin-valve magnetic trilayer,[8] and frequency dependent studies of magnetic bilayers with dissimilar dampings. Time-resolved x-ray magnetic circular dichroism (TR-XMCD) is used to sample, in a stroboscopic fashion, forced precession of elemental magnetic moments. The measurements provide extremely precise determinations of both the amplitude and phase of precessional motion during driven oscillations. Precession cone angles are measured down to 0.1° while the relative phase lag can be resolved down to ~2–5 ps (~2°–6° at 2.3 GHz).

The determination of small cone angles is enabled by the high magnetic contrast provided by transmission geometry XMCD, which is the soft x-ray analog of Faraday rotation.[9] Improved temporal resolution is achieved using phase-locked cw microwaves as an excitation source, suppressing the effects of timing jitter present in pulsed experiments. Motional and phase resolutions are an order of magnitude better than we achieved in previous work using pulsed step fields in XMCD reflectivity.[3,10]

The high sensitivity of the technique allows us to examine several aspects of magnetization precession and FMR. First, a general feature of driven resonant motion is an expected maximum in amplitude and 180° difference in phase as the driving frequency ω (or alternatively, the applied magnetic bias field H_B) passes through the resonant frequency ω_0 (H_{res}). We have verified this behavior in a time-resolved x-ray magneto-optical measurement, compared with *in situ* microwave absorption. Second, as XMCD provides element selectivity to the measurement of precessional motion, we can measure separately the response from different FM elements in our samples. In cases where the magnetic moments from these elements are bound strongly together, as is the case, for example, with the strong exchange interaction *within* a FM alloy such as $Fe_{19}Ni_{81}$, the Ni and Fe spin moments are found to be locked together in phase and amplitude within the instrumental resolution.[7] In cases where these elemental moments are bound more weakly, for example, in magnetic trilayers consisting of two FM layers separated by a nonmagnetic (NM) spacer, TR-XMCD allows us to determine extremely weak coupling between the layers.[8] In intermediate cases, such as direct coupling of dissimilar magnetic materials across a common interface, TR-XMCD reveals a

[a]Electronic mail: darena@bnl.gov

frequency dependent phase shift that develops between the layers.

The paper is organized as follows. Section II discusses the experimental details. In Sec. III, we review the theory of magnetization precession dynamics for a single particle model and apply the model to combined TR-XMCD and FMR measurements of a single $Fe_{19}Ni_{81}$ layer. The trilayer results, published previously, are reviewed in Sec. IV. Frequency dependent measurements of phase lags in magnetic bilayers are covered in Sec. V. Section VI contains preliminary measurements of precession oscillations of Tb moments in $Fe_{19}Ni_{81}$ and discusses plans for continued research into the microscopic origins of relaxation mechanisms for uniform precession modes. General conclusions are discussed in Sec. VII.

II. METHODS AND MATERIALS

Films were deposited using rf magnetron sputtering in a custom chamber with a base pressure of 4×10^{-9} torr. Transmission mode XMCD requires use of x-ray transparent films and commercially available Si_3N_4 membranes (100 nm membrane thickness) were used as the substrates. For XMCD, transmission mode has an added advantage as the signals are unaffected by applied magnetic fields. In all films, conventional XMCD spectra were recorded in helicity-switching mode at beamline 4-ID-C of the Advanced Photon Source (APS) at Argonne National Laboratory. The sample normal ($\hat{\mathbf{z}}$) was rotated ~40° with respect to the incident beam direction and the photon helicity ($\hat{\boldsymbol{\sigma}}$) had an in-plane projection along $\hat{\mathbf{y}}$. The transmitted intensity was recorded on a standard Si photodiode. All XMCD signals were normalized to a beam monitor, which consisted of the photocurrent from a Au grid placed in the beam path upstream of the sample. Element-specific hysteresis loops were acquired by tuning the photon energy to an appropriate edge (the L_3 edge of the second row transition metals and the M_5 edge of Tb), fixing the helicity of the incident beam, and sweeping the magnetic field using an *in situ* electromagnet; a component of the resulting magnetization is parallel to the photon beam direction. A complementary hysteresis loop was recorded by reversing the helicity of the incident photons and repeating the measurement. As the saturation values for the hysteresis loops correspond to a 180° change of the magnetization, they provide a convenient angular calibration for the signal levels of the time-resolved measurements.

The key to the time-resolved measurements is the use of a rf excitation that is phase locked with the arrival of photons on the samples. The rf field is generated by upconverting the APS photon bunch clock at 88 MHz to the excitation frequency. Thus the instantaneous projection of the magnetization vector along the photon beam direction is sampled stroboscopically at the same relative phase delay between the rf excitation and photon bunch clock. XMCD timing scans are generated by tuning the energy of the photons to the element of interest and incorporating a variable delay between the photon bunch clock and frequency conversion electronics. The rf excitation is amplified immediately before it is inserted into an in-vacuum, broadband microwave resonator. A hole, ~0.5 mm in diameter, in the resonator permits passage of the x-ray photons.

The experimental chamber was equipped with small electromagnet coils in a quasi-Helmholtz configuration. The coils produced a vertical field (i.e., along $\hat{\mathbf{x}}$) that was orthogonal to both the incident photon beam direction and the applied rf excitation field. The experimental apparatus could be used to measure conventional, swept-field FMR at fixed frequency. A representative scan, recorded using a small modulation on the bias field and lock-in amplification, is presented in Fig. 3(a). The *in situ* conventional FMR can be used to determine resonance fields and FMR linewidths.

III. REVIEW OF SINGLE PARTICLE THEORY AND APPLICATION TO A SINGLE $Ni_{81}Fe_{19}$ LAYER

We first describe the expected motion in a single particle model for driven ferromagnetic resonance; this model corresponds to a single precessing system or FM layer. A common starting point for analysis of magnetization dynamics is the Landau-Lifshitz (LL) equation.[11] When expressed in spherical coordinates and linearized for small-angle deviations of the magnetization $\mathbf{M}$ about the effective field $\mathbf{H}_{\text{eff}}$, the LL equation, without a forcing term, reduces to

$$\frac{\partial^2\theta}{\partial t^2}+\lambda\frac{\partial\theta}{\partial t}+\omega_0^2\theta(t)=0, \tag{1}$$

where $\omega_0^2=\mu_0^2\gamma^2H_{\text{eff}}(H_{\text{eff}}+M_s)$. Rotational displacements about an equilibrium are described by θ; ω_0 is the circular frequency of the free oscillations and $2/\lambda$ is its characteristic relaxation time. λ is the LL relaxation rate in s^{-1}, μ_0 is the vacuum permeability, γ is the gyromagnetic ratio, and M_s is the saturation magnetization. The effective field $\mathbf{H}_{\text{eff}}$, with magnitude H_{eff}, is the sum of external and internal fields in the system:

$$\mathbf{H}_{\text{eff}}=\mathbf{H_B}+\mathbf{H_K}+\mathbf{H_D}, \tag{2}$$

where $\mathbf{H_B}$ is the applied bias field, $\mathbf{H_K}$ describes the internal anisotropy, and $\mathbf{H_D}$ accounts for the demagnetization fields from shape effects.

In FMR, the motion is excited by a transverse cw driving field: $H_y(t)=H_{y0}\exp(i\omega t)$, which adds an inhomogeneous term to Eq. (1):

$$\frac{\partial^2\theta}{\partial t^2}+\lambda\frac{\partial\theta}{\partial t}+\omega_0^2\theta(t)=C\exp(i\omega t), \tag{3}$$

where $C\approx\mu_0^2\gamma^2M_sH_{y0}$. By solving Eq. (3) using $\theta(t)=\theta_0\exp(i\omega t)=|\theta_0|\exp[i(\omega t+\phi)]$, the phase ϕ and amplitude $|\theta_0|$ of driven FMR precession within a strongly coupled FM layer can be expressed as[7]

$$\tan\phi=\frac{-\lambda\omega}{(\omega_0^2-\omega^2)}, \tag{4}$$

$$|\theta_0|=\frac{C}{\sqrt{(\omega_0^2-\omega^2)^2+\lambda^2\omega^2}}. \tag{5}$$

It is worth noting that λ can be estimated directly from conventional, field swept FMR measurements:

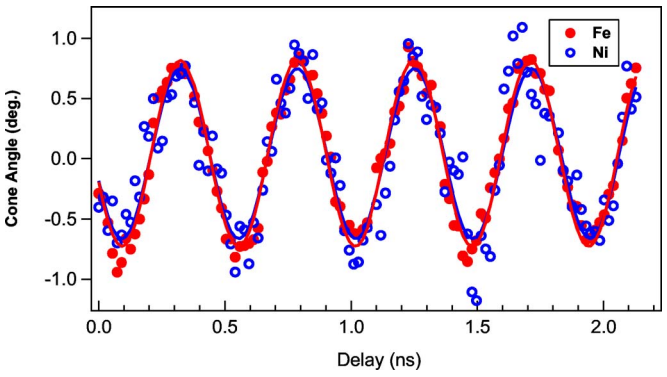

FIG. 1. (Color online) TR-XMCD measurement of Fe and Ni magnetization precessions at resonance, 37 Oe at 2.3 GHz. Solid lines are sinusoidal fits of the Fe and Ni data sets separately.

$$\lambda = \frac{\sqrt{3}}{2}\frac{\mu_0^2\gamma^2 M_s \Delta H_{pp}}{\omega}, \tag{6}$$

where ΔH_{pp} is the field spanning the inflection points in lock-in (i.e., derivative) detection of microwave absorption. In our experimental apparatus, conventional FMR is measured *in situ* and at the same frequency used for the TR-XMCD measurements. This capability permits a parameter-free comparison of the TR-XMCD data with Eqs. (4) and (5).

We first consider the single FM layer sample: 25 nm of $Ni_{81}Fe_{19}$ capped with 5 nm of Cu. Time- and element-resolved XMCD measurements of magnetization precession at resonance (H_B=37 Oe) are presented in Fig. 1. XMCD signals were taken as a function of delay time and converted into time dependent elemental magnetization angles $\theta_{Fe}(t)$ and $\theta_{Ni}(t)$ for Fe and Ni, respectively. Precessional oscillations are clearly seen. Figure 1 indicates that the Fe and Ni moments precess together, with identical phase and amplitude. At all values of H_B sampled for both elements, no difference could be detected in the motion of the Fe and Ni moments.

As expected for precessional oscillations, the delay scans show a simple sinusoidal modulation as a function of delay time. The data are fitted by a simple sine function (solid lines). The frequency is fixed by the cw microwave field at 2.3 GHz; the resulting fitted parameters for the amplitude and phase have a high degree of confidence. By combining TR-XMCD with the phase-locked cw excitation, precession amplitudes as small as 0.1° have been measured. For the strongest signals, the estimated errors in amplitude are as small as 0.02°. The phase as well can be extracted with very high precision. Estimated errors for the phase are as small as 2°–6°, or about 2–5 ps at 2.3 GHz. In contrast to our earlier measurements using pulsed excitations, the phase is determined by fitting the entire data set, rather than fitting the leading edge of a pulsed excitation. Significantly, this leads to an ensemble resolution well below the bunch length of the photons at the APS (estimated around 60 ps).

Time-resolved XMCD measurements of the driven Fe magnetization precession through the resonance curve are presented in Fig. 2. Applied fields were selected according to *in situ* measured FMR spectra [Fig. 3(a)]. The amplitude clearly increases as the bias field is swept from low values towards the resonance at ~40 Oe. A significant shift in the phase of the oscillations accompanies the growth in the amplitude.

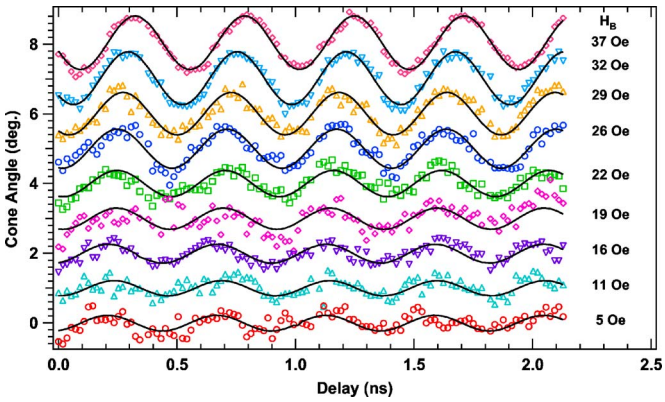

FIG. 2. (Color online) TR-XMCD measurement of Fe magnetization precession through the resonance condition. Solid lines are sinusoidal fits of each Fe data set separately. For clarity, the data are offset vertically.

A summary of the parameters extracted from the delay scans for the phase and amplitude of precession oscillations in the $Ni_{81}Fe_{19}$ layer is presented in Fig. 3(b). Also shown in the figure are simulations for the phase and amplitude from the linearized single particle model [Eqs. (4) and (5)]. λ is estimated as 1.80 GHz directly from the *in situ* measured FMR spectra [(Fig. 3(a)) using Eq. (6)]. The only empirical parameter is the strength of the driving field H_{y0}. The model is in excellent agreement with the measured values for ϕ and θ.

IV. WEAK COUPLING IN A PSEUDO-SPIN-VALVE TRILAYER

Strong exchange coupling within a FM alloy such as $Ni_{81}Fe_{19}$ binds the motion of the Fe and Ni moments together. Weak coupling, as that occurring in trilayer systems where two FM layers are separated by a NM layer, can similarly affect the precessional motion. Trilayer systems are of

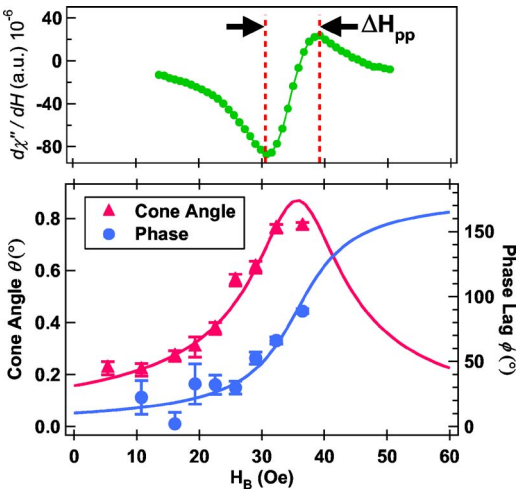

FIG. 3. (Color online) (a) In-plane FMR spectra of $Ni_{81}Fe_{19}$ measured *in situ* at 2.3 GHz. (b) Phase and precessional cone angle of Fe magnetization motion across the resonance. Solid lines are the corresponding theoretical simulations from Eqs. (4) and (5).

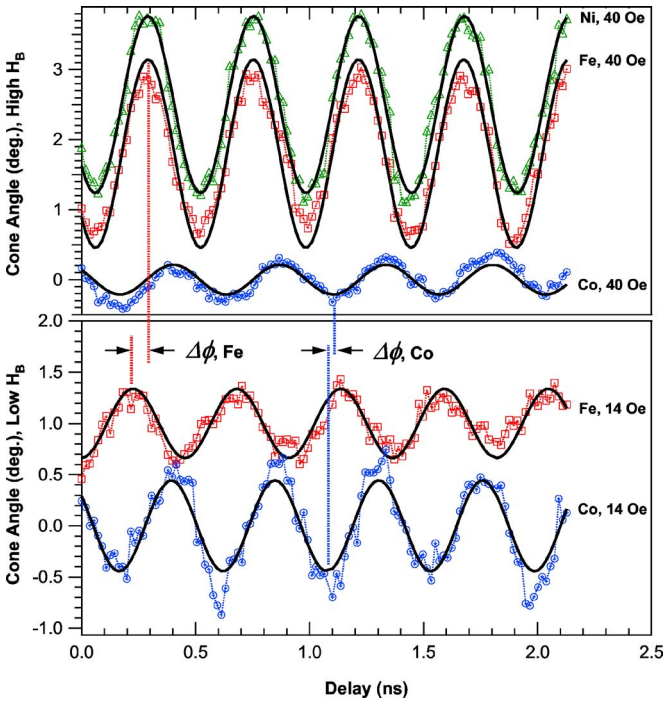

FIG. 4. (Color online) TR-XMCD measurements for Fe, Ni, and Co in the $Co_{93}Zr_7/Cu/Ni_{81}Fe_{19}$ magnetic trilayer. The open symbols are the measured points and the solid black lines are sinusoidal fits to the data. The top panel shows the response of the different layers near the main resonance at 40 Oe while the bottom panel presents the data for the low bias field condition. Note the large change in phase for the Fe oscillations ($\Delta\phi$, Fe) and the much smaller phase shift for the Co oscillations ($\Delta\phi$, Co). For clarity, the Fe and Ni data have been offset vertically.

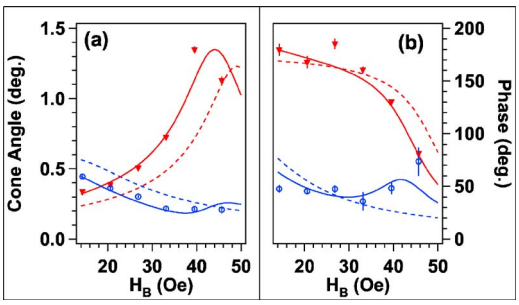

FIG. 5. (Color online) Measured values for the precession cone angle (left panel) and phase of oscillation (right panel) for the Fe (triangles) and Co (circles) moments in the $Co_{93}Zr_7/Cu/Ni_{81}Fe_{19}$ trilayer. The dashed lines are calculated values for the amplitude and phase assuming no coupling ($A_{ex}=0$) between the layers. Solid lines are model calculations that assume weak coupling ($A_{ex}=0.01$ erg/cm^2) between the two FM layers.

great importance as they form the basis for giant magnetoresistance (GMR) field sensors that underpin modern magnetic storage systems and other spintronic devices such as magnetic random access memory (MRAM). Our group has recently utilized combined TR-XMCD and FMR to investigate weak coupling in a pseudo-spin-valve trilayer consisting of $Ni_{81}Fe_{19}$ (25 nm)/Cu (20 nm)/$Co_{93}Zr_7$ (25 nm). With TR-XMCD, the effect of weak coupling on the amplitude and phase of oscillation in the individual layers is seen clearly. Figures 4 and 5 summarize the results.

Figure 4 shows the delay scans at low bias (14 Oe) and near the main resonance (40 Oe). The data indicate that the Co oscillations decrease in amplitude as the bias is increased while the phase for the Co precession ($\Delta\phi$, Co) changes very little. In contrast, the Fe amplitude grows considerably and the phase of oscillations changes by nearly 50°. The Ni oscillations, shown for $H_B=40$ Oe, are seen to copy exactly the Fe precession, again confirming the strong coupling within a FM alloy.

Figure 5 presents a summary of the phase and oscillation for the individual FM layers from low bias across the main resonance for the trilayer system; filled red triangles represent the parameters extracted for the Fe and open blue circles correspond to the Co data. The data are simulated by an extension to the single particle model where the effective field in Eq. (2) is augmented by incorporating an effective exchange field between the two FM layers:

$$\mathbf{H}_{\mathbf{ex}}^{(\mathbf{i})} = \frac{A_{\mathrm{ex}}}{\mu_0 M_s^{(i)} t^{(i)}} \frac{\mathbf{M}^{(\mathbf{j})}}{M_s^{(j)}} = \frac{A_{\mathrm{ex}}}{\mu_0 M_s^{(i)} t^{(i)}} \mathbf{m}^{(\mathbf{j})}, \tag{7}$$

where the subscript $i(j)$ indexes layer 1(2), $t^{(i)}$ is the thickness of the i^{th} layer, and A_{ex} is an effective coupling constant with units of energy per area. Also shown in Fig. 5 are numerical simulations of this two-particle model assuming no coupling between the FM layers (dashed lines) and weak coupling of 0.01 erg/cm^2 (solid lines). Assumptions of no coupling clearly overestimate the main resonance field and do not adequately describe the phase of the Fe and Co oscillations while the simulations of weak coupling provide a better match with the data. For additional information, see Ref. 8

V. FREQUENCY DEPENDENT PHASE LAGS IN AN ENGINEERED MAGNETIC BILAYER

The measurements of the trilayer structure reveal a unique aspect of TR-XMCD combined with FMR: the ability to separate the phase of oscillation of different constituents in a magnetic multilayer. This capability is quite useful in examining multilayer systems with modified, or engineered, damping. For example, the addition of a few percent of Tb into $Ni_{81}Fe_{19}$ increases the damping by close to an order of magnitude over a pure $Ni_{81}Fe_{19}$ film.[12] Magnetic bilayer structures, composed of a low damping layer adjacent to a high damping one, have been proposed as a way to engineer the overall damping in a magnetoelectronic device while preserving the spin-transport properties of the low damping layer.[13] Conventional FMR may detect a broadening of the combined resonant response, but the relative phase of oscillation between the two layers would be revealed only indirectly, through modeling of the FMR spectra.

Figure 6 presents the precessional oscillations measured in a magnetic bilayer consisting of a FM film with low damping, 25 nm of $Co_{93}Zr_7$, grown on a film with high damping, 25 nm $(Ni_{81}Fe_{19})_{99}Tb_1$. TR-XMCD measurements of precession oscillations were acquired at resonance at low frequency (1.3 GHz) and high frequency (2.3 GHz) excitations. The response of the individual layers was resolved by

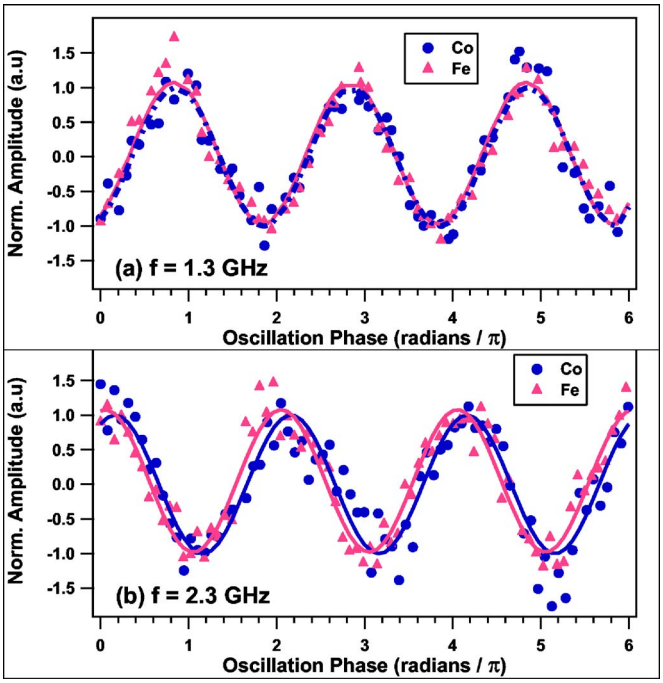

FIG. 6. (Color online) Phase lags measured for a low damping/high damping magnetic bilayer, $Co_{93}Zr_7/(Ni_{81}Fe_{19})_{99}Tb_1$, acquired at different excitation frequencies. (a) Low frequency (1.3 GHz): both layers precess in phase; (b) high frequency: the Tb doping exerts a drag on the $Ni_{81}Fe_{19}$) precessional motion and the precession lags behind the Co oscillations by ~20°. Solid lines are sinusoidal fits to the data.

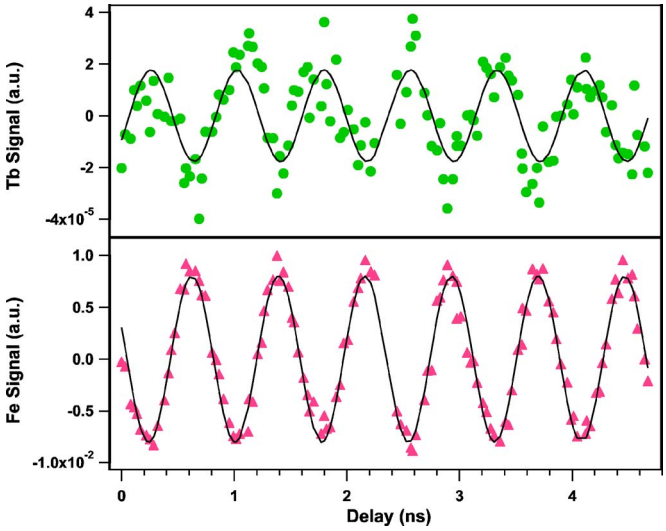

FIG. 7. (Color online) TR-XMCD measurements acquired at resonance, using an excitation frequency of 1.3 GHz, for a single $(Ni_{81}Fe_{19})_{99}Tb_1$ layer. The top layer presents the average of 41 delay scans acquired at the Tb M_5 edge while the bottom presents the oscillatory signal from a single delay scan of the Fe L_3 edge. The oscillations are primarily out of phase for the elemental moments. Solid lines are sinusoidal fits to the data.

tuning to the Fe L_3 (707.5 eV) or Co L_3 (778 eV) edges. For direct comparison, in the figure the time delay at the two frequencies is converted to oscillation phase.

At 1.3 GHz, the two layers oscillate in phase, within the experimental errors of the measurement ($\Delta\phi_{Fe-Co}=3.1°\pm4.8°$). At 2.3 GHz, a clear phase difference develops between the $(Ni_{81}Fe_{19})_{99}Tb_1$ layer and the $Co_{93}Zr_7$ layer, with the $(Ni_{81}Fe_{19})_{99}Tb_1$ lagging behind (in the figure, delay increases from left to right, and oscillation time increases from right to left). The phase lag is significant, 19.8°±6.7°, and well outside of the error in the measurement.

The TR-XCMD measurements indicate that the high damping introduced by the Tb exerts a drag on the motion of the magnetization of the Fe and Ni moments in the alloy while the Co moments are free to respond to the excitation rf field. At present, we can comment only that the results cannot be explained well by the continuum Landau-Lifshrtz-Gilbertz (LLG) models with constant exchange stiffness; in such an approach, the phase lag is expected to be proportional to resonance frequency. Modeling efforts are ongoing and additional measurements are planned.

VI. PRECESSION OF ELEMENTAL MOMENTS IN RARE-EARTH-DOPED SYSTEMS

The influence of Tb in $Ni_{81}Fe_{19}$ is clear. Tb and other rare earth (RE) dopants with nonzero orbital or total angular momentum increase the damping in soft ferromagnets.[14] In the context of RE-substituted ferrites, the microscopic origin of this increased damping is unclear. Indeed, this question has been the topic of intense speculation in the 1950s and 1960s with no clear resolution. A key aspect of most theories describing damping in RE-doped soft ferri-/ferromagnets is the relative phase between the precession of the transition metal moments and the precession of the RE moments. TR-XMCD can provide fresh insight on this topic but only if the precession signal of percent-level dopants is detectable.

Figure 7 presents the TR-XMCD signal of Fe and Tb in a $(Ni_{81}Fe_{19})_{99}Tb_1$ (100 nm) film at resonance during precession excited at 1.3 GHz. The bottom panel shows the precessional signal from a single delay scan acquired at the Fe L_3 edge. The top panel shows the average of 41 delay scans acquired at the Tb M_5 edge (1230 eV). Markers depict the data points while the solid black lines are sinusoidal fits to the data. The Fe signal exhibits a strong oscillatory signal with relatively little noise. The precessional signal associated with the Tb oscillations, on the other hand, are just above the detection limit. Nonetheless, there is a Tb oscillatory signal, and it appears to be mostly antiphase with the Fe signal. This is consistent with XMCD spectroscopy on the sample for the Fe, Ni, and Tb edges (not shown), which indicates a net antiferromagnetic (AF) alignment of the Tb with the Fe and Ni moments; however, a sperimagnetic configuration with a net AF alignment may be present.[15]

The detection of the Tb moment precession is encouraging, but the data are not sufficient yet to distinguish between the theories that have been proposed for the microscopic origins of damping in RE-doped ferromagnets. Efforts are under way to improve the efficiency of the detection of RE precession using lock-in detection, higher-power rf excitation, and lower temperatures, where phase lags are thought to be much larger.[16] Such improvements would be of use to many combined TR-XMCD and FMR experiments suffering from small signal levels.

VII. CONCLUSION

Small-angle ($<1°$) precession of elemental moments during ferromagnetic resonance in several samples has been measured by time-resolved XMCD in transmission mode synchronized with cw microwave excitation at 2.3 and 1.3 GHz. The phase and amplitude of driven FMR precession have been observed magneto-optically, with elemental resolution and great precision. The results for the single $Ni_{81}Fe_{19}$ layer are in excellent agreement with the LL equation. For the $Co_{93}Zr_7/Cu/Ni_{81}Fe_{19}$ pseudo-spin-valve structure, the TR-XMCD scans indicate dissimilar motions, in both phase and amplitude, of the two FM layers and reveal weak coupling between the FM layers. In samples with engineered damping, the TR-XMCD measurements uncover a frequency dependent phase lag that develops between a high damping layer (Tb-doped $Ni_{81}Fe_{19}$) and a low damping layer ($Co_{93}Zr_7$). Finally, TR-XMCD has been used to initiate investigations of fundamental microscopic damping mechanisms in RE-doped transition metal films via the detection of elemental phase lags in the resonant response.

ACKNOWLEDGMENTS

The authors thank David J. Keavney (APS) for beamline support. This work was partially supported by the Army Research Office with Grant No. ARO-43986-MS-YIP and the National Science Foundation with Grant No. NSF-DMR-02-39724. Use of the Advanced Photon Source was supported by the U.S. Department of Energy, Office of Science, Office of Basic Energy Sciences, under Contract No. W-31-109-Eng-38.

[1] K. Baberschke, J. Magn. Magn. Mater. **272–276**, 1130 (2004).
[2] B. Heinrich, in *Ultrathin Magnetic Structures II*, edited by J. A. C. Bland and B. Heinrich (Springer-Verlag, Berlin, 1994).
[3] W. E. Bailey, L. Cheng, E. Vescovo, C,-C. Kao, and D. A. Arena, Phys. Rev. B **70**, 172403 (2004).
[4] G. Boero, S. Rusponi, P. Bencok, R. S. Popovic, H. Brune, and P. Gambardella, Appl. Phys. Lett. **87**, 152503 (2005).
[5] J. Goulon, A. Rogalev, F. Wilhelm, N. Jaouen, C. Goulon-Ginet, G. Goujon, J. Ben Youssef, and M. V. Indenbom, JETP Lett. **82**, 969 (2005).
[6] A. Puzic *et al.*, J. Appl. Phys. **97**, 10E704 (2005).
[7] Y. Guan, W. E. Bailey, E. Vescovo, C.-C. Kao, and D. A. Arena, J. Magn. Magn. Mater. **312**, 374 (2007).
[8] D. A. Arena, E. Vescovo, C.-C. Kao, Y. Guan, and W. E. Bailey, Phys. Rev. B **74**, 064409 (2006).
[9] C. T. Chen, Y. U. Idzerda, H. J. Lin, N. V. Smith, G. Meigs, E. Chaban, G. H. Ho, E. Pellegrin, and F. Sette, Phys. Rev. Lett. **75**, 152 (1995).
[10] Y. Guan, W. E. Bailey, C.-C. Kao, E. Vescovo, and D. A. Arena, J. Appl. Phys. **99**, 08J305 (2006).
[11] L. D. Landau, E. M. Lifshitz, and L. P. Pitaevski, *Statistical Physics* (Pergamon, Oxford, 1980), Pt. 2.
[12] W. Bailey, P. Kabos, F. Mancoff, and S. Russek, IEEE Trans. Magn. **37**, 1749 (2001).
[13] H. Song, L. Cheng, and W. E. Bailey, J. Appl. Phys. **95**, 6592 (2004).
[14] S. G. Reidy, L. Cheng, and W. E. Bailey, Appl. Phys. Lett. **82**, 1254 (2003).
[15] Y. Guan, Z. Dios, D. A. Arena, L. Cheng, and W. E. Bailey, J. Appl. Phys. **97**, 10A719 (2005).
[16] M. Sparks, *Ferromagnetic Relaxation Theory* (McGraw-Hill, New York, 1965).